AGU PUBLICATIONS

JGR

Journal of Geophysical Research: Space Physics

RESEARCH ARTICLE
10.1002/2016JA023498

Disturbance dynamo effects over low-latitude *F* region: A study by network of VHF spaced receivers

B. Kakad[1], **G. Surve**[1], **P. Tiwari**[1], **V. Yadav**[1], **and A. Bhattacharyya**[1]

[1] Indian Institute of Geomagnetism, Navi Mumbai, India

Key Points:
- Magnetic activity (MA) effects on *F* region zonal irregularity drifts are marginally higher at equator
- Effect of MA on low-latitude *F* region zonal irregularity drifts are stronger, when $\Delta T < 4$ h
- LSWS-linked variability in the occurrence of fresh ESF is seen within a longitudinal belt of 5.6°

Correspondence to:
B. Kakad,
ebharati@iigs.iigm.res.in

Citation:
Kakad, B., G. Surve, P. Tiwari, V. Yadav, and A. Bhattacharyya (2017), Disturbance dynamo effects over low-latitude *F* region: A study by network of VHF spaced receivers, *J. Geophys. Res. Space Physics*, *122*, doi:10.1002/2016JA023498.

Received 21 SEP 2016
Accepted 9 MAY 2017
Accepted article online 15 MAY 2017

Abstract Generation of equatorial spread *F* (ESF) irregularities resulting from magnetic disturbance is known for past few decades. However, better prediction models for this phenomenon are still lacking. Magnetic storms also affects the *F* region plasma drifts. In this work we examined variability in (i) occurrence of such freshly generated ESF and (ii) low-latitude *F* region zonal plasma drifts over Indian longitude. For this purpose simultaneous observations of amplitude scintillations on 251 MHz signal, recorded by a network of spaced receivers located at low-latitude stations, are utilized. Observational stations are situated such that it longitudinally (latitudinally) covers an area of 5.6° (13°). Here effect of disturbance dynamo (DD) electric field at low-latitude *F* region and its variability are studied for three magnetic storms occurring in 2011. These magnetic storms are having nearly similar type characteristics except their start time. We find that as time difference (i.e., ΔT) between local sunset and start of magnetic activity decreases, the DD effects seen at low-latitude *F* region zonal irregularity drift around midnight becomes stronger. For a given magnetic storm the DD effect on *F* region zonal irregularity drifts is found to be only marginally stronger at dip equator in comparison to off-equatorial stations. Although effect of DD on *F* region zonal irregularity drifts are felt simultaneously, generation of fresh ESF is variable within a smaller longitudinal belt of 5.6°. It is attributed to the presence of LSWS at the bottomside of *F* region, as initiation of ESF is highly likely (unlikely) in the vicinity of crest (trough) of such LSWS.

1. Introduction

Nonlinear evolution of Rayleigh-Taylor (RT) plasma instability at the equatorial *F* region during postsunset hours results in electron density irregularities, known as equatorial spread *F* (ESF). These ESF irregularities vary from few centimeters to hundreds of kilometers and produce amplitude and phase scintillations on radio signal traversing through them. Information on spatial scales of ESF irregularities are of great interest as small-scale fast-moving irregularities are likely to cause more degradation to the incoming radio signal. Spaced receiver scintillation technique is an effective way to retrieve information about the equatorial plasma bubbles (EPBs) and associated ESF irregularities. This technique is in use from past many years [*Wernik et al.*, 1983; *Bhattacharyya et al.*, 1989, 2001; *Basu et al.*, 1991; *Valladares et al.*, 1996, 2002; *Kil et al.*, 2002; *Ledvina et al.*, 2004]. Observational and theoretical studies have shown that the postsunset height of *F* region, background magnetic field, alignment of sunset terminator with magnetic meridian, and *E* region zonal conductivity gradients at conjugate points play an important role in setting the favorable conditions for the RT plasma instability [*Heelis et al.*, 1974; *Tsunoda*, 1985; *Abdu et al.*, 1992; *Park et al.*, 2010]. *Joshi et al.* [2013a, 2013b] have reported that the *E* region integrated conductivity influences the growth of the RT plasma instability. In spite of these favorable conditions, a seeding perturbation is vital for the initiation of large-scale RT plasma instability, which is sometimes provided by gravity waves [*Tsunoda*, 2012; *Krall et al.*, 2013]. Simulation studies by *Huang and Kelley* [1996] have shown that the spatially varying electric field can generate EPBs. The periodic electric fields generated by gravity waves in the off-equatorial *E* region mapped into the equatorial *F* region along the magnetic field lines can be likely source for such electric fields. The presence of large-scale wave structure (LSWS) at the bottomside of the *F* region is considered as early manifestation for such seed perturbation [*Kelley et al.*, 1981; *Tulasi Ram et al.*, 2014; *Zhu et al.*, 2015; *Joshi et al.*, 2015]. These LSWS can also serve as a source for such spatially varying electric fields. Studies have shown that the occurrence of EPBs varies with solar flux, seasons, magnetic activity, longitude, and latitude [*Burke et al.*, 2004; *Nishioka et al.*, 2008]. However, the day-to-day occurrence of EPBs is still an open question in terms of prediction.

Generation of EPBs is either triggered or suppressed due to magnetic activity-linked electric fields [*Abdu et al.*, 1997; *Sastri*, 1999; *Martinis et al.*, 2005]. Effects of magnetic activity observed at equatorial *F* region are associated with either disturbance dynamo (DD) electric field or prompt penetration (PP) of magnetospheric electric field [*Blanc and Richmond*, 1980; *Spiro et al.*, 1988; *Fejer et al.*, 1990]. Sometimes the observed effect can be a consequence of both DD and PP electric fields [*Maruyama et al.*, 2005; *Kakad et al.*, 2007]. Turning of background electric field from west-east due to superimposed disturbed time electric field raises the equatorial *F* region to higher altitudes, where RT plasma instability can be initiated with appropriate seeding perturbation to give rise to EPBs. *Kakad et al.* [2007] have examined the occurrence of magnetic activity-linked freshly generated EPBs at a single equatorial station in the Indian longitude. They have shown that such freshly generated ESF irregularities are prevalent close to local midnight. Generation of ESF irregularities requires eastward electric field that can raise the *F* region to higher altitude, where ambient ionospheric conditions are favorable for the growth of RT plasma instability. Simulation studies have reported the westward to eastward turning of disturbed time electric field around midnight with some longitudinal variability [*Richmond et al.*, 2003; *Huang et al.*, 2005]. It is important to note that presence of LSWS can contribute positively (negatively) to the ambient zonal electric field in regions of crest (trough) of these structures [*Tsunoda*, 2005] and hence play an important role in the genesis of equatorial EPBs and associated irregularities.

It is well know that sometimes the ESF irregularities are freshly generated as a result of magnetic activity [*Kakad et al.*, 2007, 2012]. Yet we are far from the predictions of such freshly generated ESF. The question here is, can we predict occurrences of such freshly generated ESF irregularities by relating it to some of the characteristics of magnetic storms? Other major effect is linked with the modulation of ambient zonal plasma drifts due to disturbed time electric fields and neutral winds. The latitudinal variation of effect of magnetic disturbance on low-latitude *F* region zonal plasma drifts is not well explored. In such study, it is essential to quantify the "cause" and "effect" both for similar-type events to get reliable predictions. In the present study, we have selected three "near-similar-type" magnetic storms having different start time and investigated the longitudinal variability of their effects at low-latitude *F* region in the postsunset hours. We have made an attempt to quantify both the "cause" (magnetic storm) and "effect" (disturbances in *F* region) for these magnetic storms. To the best of our knowledge this is the first study carried out using the simultaneous observation of VHF amplitude scintillations recorded by network of spaced receivers at low-latitude stations in the Indian longitude. VHF scintillation network and data used in the present study are described in section 2. Data analysis technique is briefed in section 3. The characteristics of magnetic storms and the reason for considering them under near-similar-type category are elaborated in section 4. The effects of DD electric field observed at low-latitude *F* region are discussed in section 5, separately for each magnetic storm. The physical explanation for the observed effects is discussed in section 6. The present work is summarized and concluded in section 7.

2. VHF Scintillation Spaced-Receiver Network and Data Utilization

Intermediate scale size (100 m to few kilometers) ESF irregularities cause scintillations on VHF signal. We use amplitude scintillations on 251 MHz signal transmitted from geostationary satellite UFO10 (72.4°E) and recorded by network of spaced receivers at low-latitude stations during 2011. The spaced receivers are closely aligned along the magnetic E-W at stations, namely, Tirunelveli (8.7°N, 77.8°E, dip latitude 1.5°N), Gadanki (13.5°N, 79.2°E, dip latitude 7.3°N), and Kolhapur (16.7°N, 74.3°E, dip latitude 10.4°N). A single receiver amplitude scintillations on the same frequency recorded at Mumbai (19.09°N, 72.9°E, dip latitude 14.5°N) and CADI ionosonde data recorded at Tirunelveli are also utilized. The zenith angle θ, azimuth angle A of the signal path transmitted from UFO10 at above mentioned stations are Tirunelveli 12.8° and 216.9°, Gadanki 18.34° and 210°, and Kolhapur 19.89° and 190.2°, respectively. The distance between two receivers x_0 at these stations are 540 m, 410 m, and 265 m, respectively. Sampling frequency of amplitude scintillations is 20 Hz.

The location of these stations on map of India is shown in Figure 1a. It is important to note that the observation stations do not lie in the same magnetic longitude. The geographic latitude, geographic longitude, dip latitude, and magnetic longitude of these stations are given in Table 1. The location of these stations are such that longitudinally it covers 5.6° (i.e., 654 km at an altitude of 300 km), and latitudinally, it spans 13° (i.e., 1520 km at an altitude of 300 km). The interstation longitudinal separation for Mumbai-Kolhapur, Kolhapur-Tirunelveli, and Tirunelveli-Gadanki are 1.1°, 2.66°, and 1.8°, respectively. It is reasonable to assume Mumbai (geomagnetic longitude 146.6°E) and Kolhapur (geomagnetic longitude 147.7°E) on the same magnetic longitude as they are separated by relatively smaller distance ($\approx$ 1.1°). We have named this magnetic longitude as L_A,

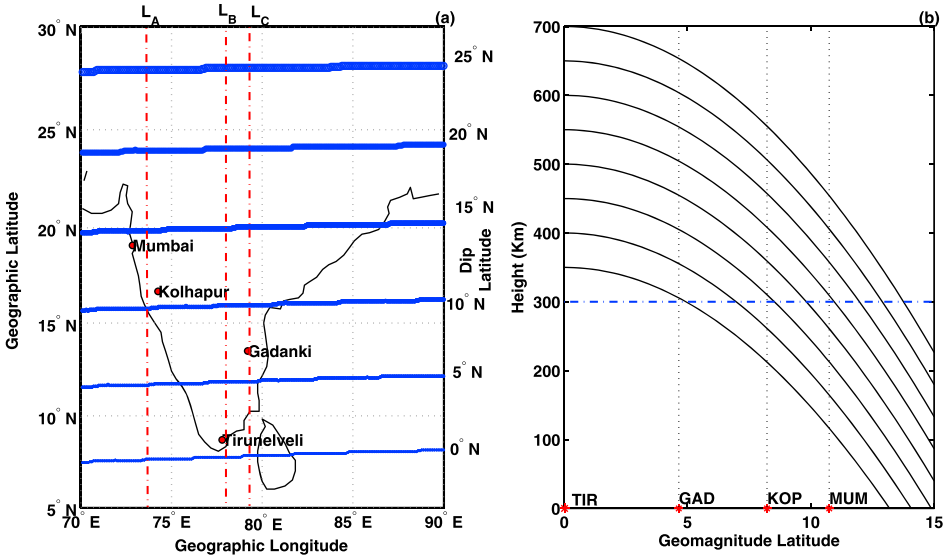

Figure 1. (a) The location of observation stations in Indian region. These observation stations are situated closely on three magnetic longitude L_A, L_B, and L_C covering 5.6°, i.e., 652 km at an altitude of 300 km. (b) Demonstrates the path followed by magnetic field lines as a function of altitude and magnetic latitude.

and it is considered at $(L_{MUM} + L_{KOP})/2 = 147.15°$. On the other hand, Tirunelveli (geomagnetic longitude 150.4°E) and Gadanki (geomagnetic longitude 152.2°E) are considered on separate magnetic longitude, namely, L_B and L_C. These three longitudes are marked in Figure 1a by vertical red dash-dotted lines.

The magnetic field lines are represented by $r = L\cos^2(\Psi)$, where L is the equatorial crossing point of the magnetic field line and Ψ is the magnetic latitude [*Kelley*, 1989]. The path followed by magnetic field lines with different apex altitudes over the magnetic equator are displayed in Figure 1b. ESF irregularities are magnetic field aligned, due to high conductance along the direction parallel to the magnetic field. Figure 1b indicates that the ESF irregularities situated at an altitude of ~541 km, 440 km, and 344 km over the magnetic equator can map down to Mumbai, Kolhapur, and Gandanki at ~300 km, respectively. These altitudes (Z_{dip}) are given in Table 1. The altitude of ESF irregularity over magnetic equator is important parameter that decides the latitudinal extent of the spread *F*. Smaller spatial scale ESF irregularities situated above *F* peak maps down to Mumbai and produces stronger VHF/L band scintillation there due to higher ambient electron density in the equatorial anomaly region [*Bhattacharyya et al.*, 2014, 2017]. Thus, if we have scintillation observations at chain of low-latitude stations located closely along the same magnetic longitude, then a meaningful information can be drawn regarding altitudinal extent of the ESF irregularities and their mapping to low-latitude stations. Also, if such observations are available in different magnetic longitudes (i.e., L_A, L_B, and L_C), then longitudinal variability of occurrence of the EPBs can be examined. Most importantly, such network of spaced receivers is useful to study the latitudinal variation in nighttime *F* region zonal plasma drifts during magnetically disturbed periods over a given longitudinal belt.

Table 1. Geographic Latitude, Geographic Longitude, Magnetic Longitude, and Dip Latitude of Observation Stations[a]

	MUM	KOP	TIR	GAD
Geographic latitude	19.1°N	16.7°N	8.7°N	1.5°N
Geographic longitude	72.9°E	74.3°E	77.8°E	79.2°E
Geomagnetic longitude	146.6°E	147.7°E	150.4°E	152.2°E
Dip latitude	14.5°N	10.4°N	1.5°N	7.3°N
Z_{dip}	541 km	440 km	—	344 km

[a]ESF irregularities located at an altitude of Z_{dip} over magnetic equator maps down to these observation stations at an altitude of 300 km.

3. Data Analysis Technique

Spaced receiver scintillations recorded at each station are analyzed using full cross-correlation technique [*Brigg*, 1984], and parameters S_4, V_0, V_C, and $C_l(x_0, t_m)$ are computed for every 3 min. S_4 gives information about strength of scintillation, and random velocity V_C is the measure of random changes in the irregularity characteristics. V_0 is the drift of the ground scintillation pattern in the receivers plane, which is determined by the drift of the irregularities across signal path. $C_l(x_0, t_m)$ is the maximum cross-correlation between intensity variations recorded by two receivers. In the analysis the space-time correlation function of intensity is assumed to have a form of $C_l(x, t) = f[(x - V_0 t)^2 + V_C^2 t^2]$, where function f is monotonically decreasing function of its argument [*Engavale et al.*, 2005]. The assumed functional form of f has greater validity when maximum correlation between two signals is larger than or equal to 0.5 (i.e., $C_l(x_0, t_m) \geq 0.5$). Hence, V_0 and V_C are estimated in this regime. It should be noted that incoming radio signal has nonzero zenith and azimuth angle. Thus, V_0 provides the average of projection of irregularity drift transverse to signal path, in receivers plane. Considering the geometry of the incoming radio signal, we get $V_0 = V_X - V_Z \tan\theta \sin A$, where V_X and V_Z are eastward and vertical drift of irregularities. Substitution of zenith and azimuth of a signal path in above expression indicates that $-0.13V_Z$, $-0.17V_Z$, and $-0.06V_Z$ contributes to V_0 at Tirunelveli, Gadanki, and Kolhapur, respectively. The vertical drift of irregularity is smaller after 22:00 LT, and hence, its contribution to V_0 can be neglected. It is established that the estimated V_0 can be considered as representative of background zonal plasma drift after 22:00 LT [*Basu et al.*, 1996; *Valladares et al.*, 1996; *Retterer*, 1999; *Bhattacharyya et al.*, 2001]. The other important parameter is the $C_l(x_0, t_m)$, which is used to identify the fresh generation of ESF irregularities resulting from magnetic activity [*Bhattacharyya et al.*, 2002].

ESF irregularities follow a power law spectrum, i.e., $\Phi(\Delta N) \propto k^{-p}$, where p is three-dimensional power spectral index. This power law nature of spectrum is bounded by inner r_0 and outer scale R_0 [*Yeh and Liu*, 1982]. According to weak scintillation theory, the ESF irregularities having scale size of the order of Fresnel scale (d_F) contribute maximum to the weak amplitude scintillations. The broad maximum seen in the power spectrum represents Fresnel frequency ν_F, and it can be converted to Fresnel scale with the knowledge of drift speed of irregularity, i.e., $d_F = V_0/\nu_F$ [*Wernik et al.*, 1983; *Kakad et al.*, 2012]. When irregularity layer is sufficiently thin and phase fluctuations imposed on incoming radio wave have standard deviation smaller than unity (i.e., $\sigma_\phi^2 << 1$), Fresnel oscillations are likely to be present in the spectrum for such cases. The frequencies associated with nth Fresnel maximum and minimum are given by $\nu_{Fn} = \sqrt{(2n-1)V_0^2/2\lambda Z}$ and $\sqrt{nV_0^2/\lambda Z}$, respectively, where Z is the average vertical distance of irregularity layer from receiver, and λ is the wavelength of incoming radio signal. Here $n = 1, 2, 3$ represents the position of the maximum/minimum. Above mentioned expressions for the Fresnel frequency indicate that the Fresnel frequency (ν_{Fn}) obtained through power spectral analysis can be used to get the height of the irregularity layer when information on drift speed of irregularity (V_0) is known. The power spectral analysis can be carried out only for the weak scintillations as power spectrum is extended to higher frequencies for strong scintillations. In the present study, we have estimated the irregularity height using the frequency linked with the first ($n = 1$) Fresnel maxima.

4. Magnetically Disturbed Days

Generally, each magnetic storm is different from the other. In order to have better prediction models for magnetic activity-related effects at F region, it is a good idea to investigate these effects statistically for nearly similar magnetic storms. However, the selection of "similar-type" magnetic storm is not straightforward due to complexities involved in the phenomenon. It is important to note that each magnetic storm is different from the other as their sources, characteristics, strength, start time, and time variation are different from one another. In such a situation it is reasonable to identify magnetic storm having characteristics in the close range so that statistically we can treat these magnetic storms under "near-similar-type" category. We have considered three magnetic storms that occurred on 17 September, 6 April, and 9 September during 2011. To claim these magnetic storms as "near-similar," we followed two steps. First, we noted the characteristics of various parameters linked with magnetic activity and then estimated the Joule energy deposited at high latitudes. Geomagnetic indices like *SYM-H*, *AE*, *ap*, and interplanetary parameters used in the present study are obtained from http://wdc.kugi.kyoto-u.ac.jp/ and http://cdaweb.sci.gsfc.nasa.gov/index.html/.

Figure 2 shows the magnetic activity indices *SYM-H* and *ap* as a function of Indian standard time (IST) for above mentioned magnetically disturbed days. To maintain the same time frame, all the plots discussed in this paper are displayed in Indian standard time (IST). Here $LT_{\text{Tirunelveli}} = \text{IST} - 0.31$, $LT_{\text{Gadanki}} = \text{IST} - 0.22$,

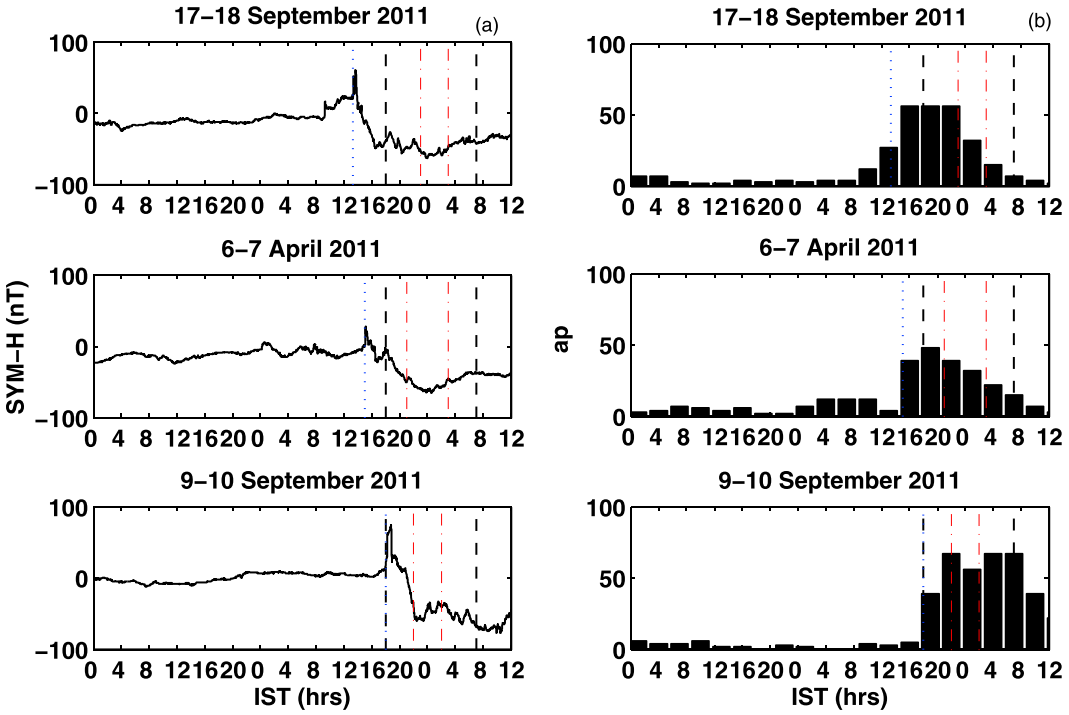

Figure 2. Variation of magnetic activity indices (a) *SYM-H* and (b) *ap* as a function of IST. These indices are shown from 00 IST of previous day of magnetically disturbed days: (i) 17 September 2011, (ii) 6 April 2011, and (iii) 9 September 2011. Vertical black dashed line represents the postsunset period from 18 to 6 h, when magnetic activity effects are examined at low-latitude *F* region. Vertical red dash-dotted line shows the time when magnetic activity-linked effects are observed at longitude L_A or L_B, or L_C, or all. The start time of magnetic activity is shown by blue dotted vertical line.

and $LT_{\text{Kolhapur}} = \text{IST} - 0.55$. It should be noted that the variation of *SYM-H* and *ap* is plotted from 00 IST of previous day of the magnetically disturbed day considered for the study. We investigate the effect of magnetic activity at low-latitude *F* region in the postsunset hours, i.e., ≈ 18 LT to 06 LT of the next day, which is indicated by vertical dashed line in Figure 2. It is evident that these magnetically disturbed days are preceded by magnetically quiet conditions, and corresponding *ap* and *SYM-H* variations are found to be $ap < 7$ and -25 nT $< SYM\text{-}H < 10$ nT, respectively. This ensures that the effects observed over low-latitude *F* region on these 3 days are linked with the magnetic activity occurring on the same day. Vertical dash-dotted red lines indicate the period T_{effect}, when magnetic activity-linked effects are evident at low-latitude *F* region in longitude L_A or L_B or L_C. It is found that these effects are seen between 21 and 03 IST, with maximum impression around 00 IST.

Here we take sudden increase in *SYM-H*, which represents storm sudden commencement as a start time for the magnetic activity, T_D. For 17 September, 6 April, and 9 September, the magnetic activity initiated at 13.3 IST, 15 IST, and 18 IST, respectively, which is shown by vertical blue dotted line in Figure 2. The corresponding variation of IMF-B_z and its time rate of change over 15 min are shown in Figure 3. To compare these magnetic storms, we have noted their characteristics, viz., minimum *SYM-H*, minimum IMF-B_z, minimum rate of change of IMF-B_z, and minimum rate of change of *SYM-H* and it is given in Table 2. It is clear from Table 2 that the characteristics of magnetic storms are in close range with some variability. It may be noted that the start time for each magnetic storm is different. Thus, for each magnetic storm the variation of *SYM-H* and *AE* with time *T* is considered as a function of the shifted time $(T - T_D)$ such that the start time of magnetic activity for each event coincides with $T - T_D = 00$ h. These variations are shown in Figures 4a and 4b for comparison. Vertical gray dashed line in Figures 4a–4c represents $T - T_D = 00$ h.

As a second step, we computed Joule energy deposited at high latitudes starting from their shifted start time (i.e., 00 h). For this purpose we estimated the power by using empirical formula given by *Akasofu* [1981], which utilizes the *AE* indices. Joule energy computation involves the integration of the power from start time t_1 to end time t_2. Here we have taken $t_1 = 00$ and varied t_2 from 0 to 15 h at the interval of every 30 min.

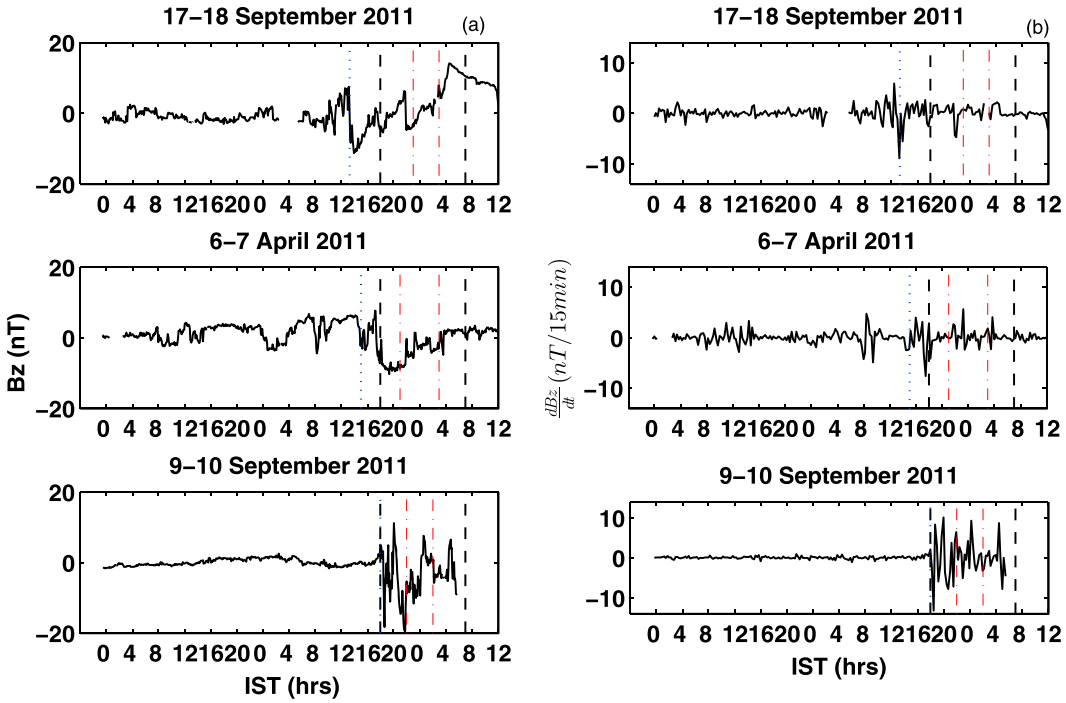

Figure 3. (a) IMF B_z and (b) its rate of change are shown as a function of IST for (i) 17 September 2011, (ii) 6 April 2011, and (iii) 9 September 2011. Vertical black dashed line shows the postsunset period from 18 to 6 h, when magnetic activity effects are examined at low-latitude F region. Vertical red dash-dotted line represents the period when magnetic activity-linked effects are observed at longitude L_A or L_B, or L_C, or all. The start time of magnetic activity is shown by blue dotted vertical line.

The average Joule energy (E_{t2}^{t1}) deposited at high latitudes from the start time of magnetic activity is shown in Figure 4c as a function of time duration, $T - T_D$. Joule energies deposited at high latitudes play an important role in the development of disturbance dynamo (DD). It should be noted that the maximum deviation in zonal irregularity drift is observed at time $T_{\max} = 23.75$ IST, 23.6 IST, and 01 IST, respectively, for 17–18 September, 6–7 April, and 9–10 September 2011, and their details are briefed in section 5. The vertical dash-dotted line shown in Figure 4c indicates the time $T_{\max} - T_D$ in hours for these three events. Joule energy deposited over the period of $t_1 = 00$ to $t_2 = T_{\max} - T_D$ is given by $E_{t2=T_{\max}-T_D}^{t1=00}$ and found to be 4.25e15 J, 3.54e15 J, and 3.70e15 J, respectively, for these magnetic storms. It is clearly evident that average Joule energies deposited at high latitudes after initiation of magnetic activity are following similar trend and are in approximately same range. As the characteristics of these magnetic storm and Joule energy inputs at high latitudes are in close range, it is reasonable to treat these magnetic storms under nearly similar-type domain.

Table 2. List of the Various Parameters Considered to Characterize the Magnetic Storm

	17–18 September 2011	6–7 April 2011	9–10 September 2011
$SYM\text{-}H_{\min}$	−57 nT	−59 nT	−62 nT
$B_{z_{\min}}$	−11.2 nT	−10.3 nT	−18.3 nT
$\frac{dB_z}{dt}\|_{\min}$	−8.5 nT/15 min	−7.8 nT/15 min	−13 nT/15 min
$\frac{dSYM\text{-}H}{dt}\|_{\min}$	−30 nT/10 min	−15 nT/10 min	−40 nT/10 min
T_D	13.3 IST	15.03 IST	18.0 IST
T_{effect}	23–03 IST	21–03 IST	22–02 IST
$T_{\max}$	23.75 IST	00 IST	01 IST
$E_{t_2=T_{\max}-T_D}^{t_1=00}$	4.25e15 J	3.54e15J	3.70e15J
$\Delta T = T_{\langle T_{sunset}\rangle} - T_D$	4.7 h	3.0 h	00 h

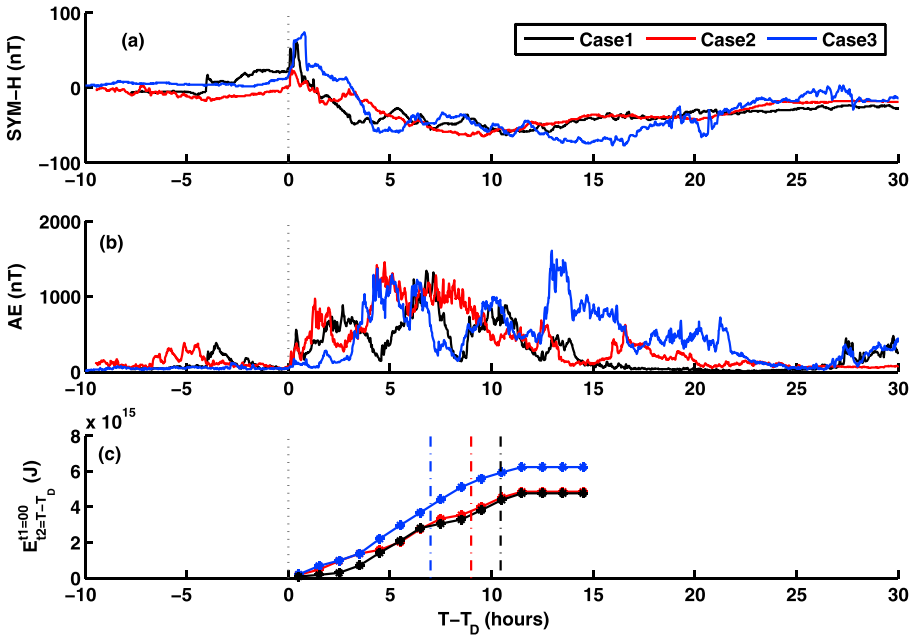

Figure 4. Time shifted variation of (a) *SYM-H* and (b) *AE* are shown for 17 September 2011, 6 April 2011, and 9 September 2011. Here $T - T_D = 00$ h represent the start time of each magnetic storm, which is marked by vertical gray dashed line in Figures 4a–4c. (c) The average Joule energy, E_{t2}^{t1} deposited at high latitudes during period starting from the time $t_1 = 00$ to $t_2 = T - T_D$ is shown as a function of time duration, $T - T_D$. Dash-dotted vertical lines in Figure 4c represent the time, when maximum deviation is observed in the zonal plasma drift (i.e., T_{max}) for respective magnetic storm.

The effect of DD at low-latitude ionosphere can be seen within less than a few hours (short period) or after few tens of hours (long period). *Scherliess and Fejer* [1997] have shown that on average, DD process are associated with time delays of about 1–12 h and 22–28 h. Recently, *Kakad et al.* [2011] studied the short- and long-period DD effects at low-latitude *F* region and reported the time delays of 0.5–4 h and 16–23 h for high solar flux period. One can note that the maximum effects of the magnetic disturbance on the low-latitude ionosphere are being observed approximately 4–10 h after its initiation for the cases studied here. It suggests that the effects presented here are associated with short-time DD.

5. Results

It is known that for magnetically quiet nights, estimated V_0 follow a well-defined pattern after 22:00 LT for a given month. But on magnetically disturbed days, estimated V_0 can show significant departure from their monthly quiet time average zonal irregularity drifts [*Bhattacharyya et al.*, 2002; *Kakad et al.*, 2012]. Also, it is reported that the parameter $C_I(x_0, t_m)$ can be used effectively to identify the fresh generation of ESF irregularities resulting from magnetic activity [*Bhattacharyya et al.*, 2002]. It may be noted that such freshly generated EPBs can be identified only when perturbation electric field associated with usual RT instability is eroded, i.e., ~ after 22 LT. Because before 22 LT, there may be postsunset freshly generated EPBs due to PREs as in the case of magnetically quiet days. Thus, here we investigate the effect of magnetic activity on (i) zonal irregularity drift V_0 and (ii) fresh generation of EPBs at low-latitude *F* region during the postsunset hours using scintillation data recorded by network of spaced receivers. Although longitudinal separation between stations considered under category "A," "B," and "C" is small, ≈1.8–3.25°, it is worthwhile to investigate the variation in the effects associated with magnetic activity over these magnetic longitudes, as it covers a distance of nearly 210–380 km (at an altitude of 300 km), which is larger as compared to average bubble size of 70 km [*Yeh et al.*, 1979].

It should be noted that the base height of *F* region obtained from ionosonde observations is available only in longitude L_B. As we are examining the magnetic activity-linked genesis of EPBs around postmidnight hours over a narrow longitudinal belt of width 5.6°, we can assume variation of $h'F$ at L_A and L_C to be of similar type to that at L_B. It is because the DD electric field is not expected to change drastically over such a narrow longitudinal zone. However, it is worth noting that the presence of LSWS can increase/decrease $h'F$ by 50–100 km, which is of the order of vertical scale size of LSWS. Although, we do not have observation at the dip equator

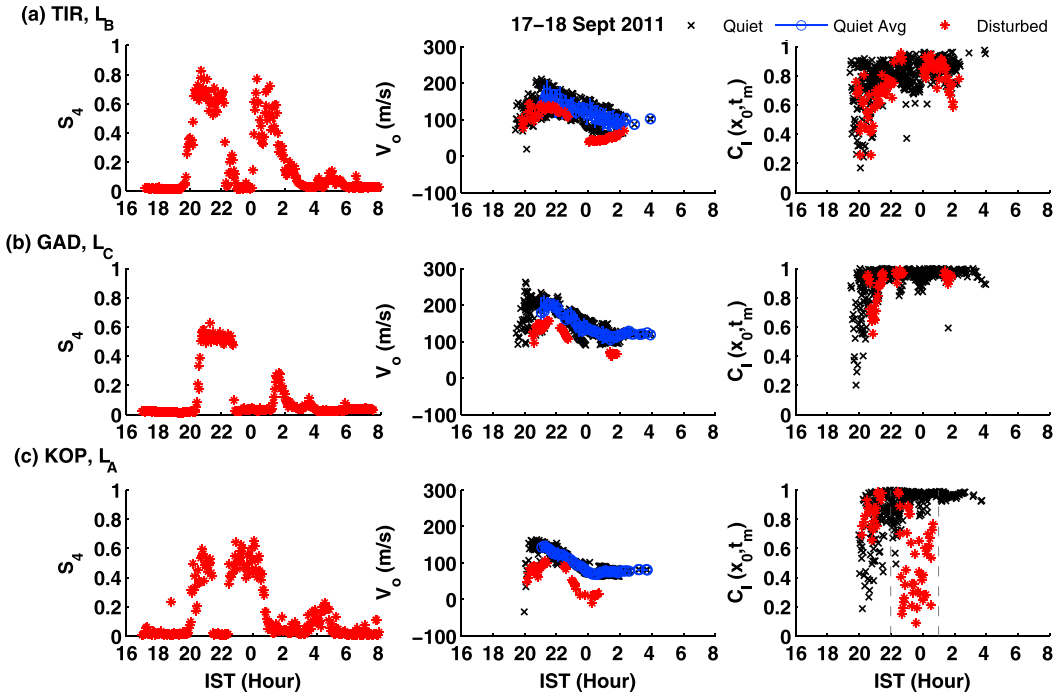

Figure 5. (left column) S_4; (middle column) quiet (black) and disturbed (red) time V_0, along with corresponding monthly quiet time average of V_0 (blue); (right column) quiet (black) and disturbed (red) time $C_I(x_0, t_m)$, as a function of IST for 17–18 September at observation stations (a) Tirunelveli, L_B; (b) Gadanki, L_C; and (c)Kolhapur, L_A.

on longitude L_A and L_C, we can still confirm the fresh generation of EPBs at these longitudes using $C_I(x_0, t_m)$ from off-equatorial stations Kolhapur and Gadanki. If ESF irregularities are generated freshly as a result of magnetic activity at dip equator on longitude L_A (L_C), then they can map to Kolhapur/Mumbai (Gadanki) through magnetic field lines, when their altitude at dip equator is around 440/541 km (344 km). Thus, the signature of freshly generated ESF irregularities can be identified at off-equatorial stations as well. Here we explain the longitudinal variability of the effects linked with short-time DD at low-latitude Indian stations for three near-similar-type magnetic storms.

5.1. Case 1: 17–18 September 2011

Figure 5 shows the S_4, V_0, and $C_I(x_0, t_m)$ observed at (a) Tirunelveli, L_B; (b) Gadanki, L_C; and (c) Kolhapur, L_A for 17–18 September 2011. Quiet time variation of V_0 and $C_I(x_0, t_m)$ are shown by black cross superposed with disturbed time variation with red asterisk. The quiet time average pattern of V_0 is shown by blue circles with error bars. Generally, the signals from both receivers are highly decorrelated in the early phase of evolution of RT instability resulting in lower values of $C_I(x_0, t_m)$. However, when perturbation electric field associated with RT instability is eroded, the $C_I(x_0, t_m)$ is found to be higher. This feature is consistent and evident from last vertical panel of Figure 5. On magnetically disturbed days the lower (<0.5) values of $C_I(x_0, t_m)$ are found even after 22 LT, which indicates the fresh generation of ESF [*Kakad et al.*, 2007]. It is noted that such decrease in $C_I(x_0, t_m)$ is observed only at Kolhapur, indicating the presence of freshly generated ESF irregularities at dip equatorial station on longitude A. As this freshly generated ESF irregularities are at appropriate altitude ($\geq$ 440 km), they are mapped to off-equatorial station through magnetic field line and hence we observe lower $C_I(x_0, t_m)$ at Kolhapur during 22–01 IST. This freshly generated ESF is shown by dashed vertical lines in Figure 5c. On the other hand, we do not observe fresh generation of EPBs at stations situated on longitude B and longitude C (Tirunelveli and Gadanki). It indicates that the fresh generation of ESF is triggered only at L_A and not at L_B and L_C which are, respectively, 3.2° and 5° away from L_A.

Furthermore, at all these stations the disturbed time irregularity drift V_0 displayed a clear departure from their monthly quiet time variability that can be seen in Figure 5 (middle column). On disturbed days, sometimes the short-duration gaps are seen in V_0, V_C, and $C_I(x_0, t_m)$ that are linked with no scintillations. These gaps are encountered as meaningful information cannot be retrieved from correlation analysis when $S_4 < 0.15$.

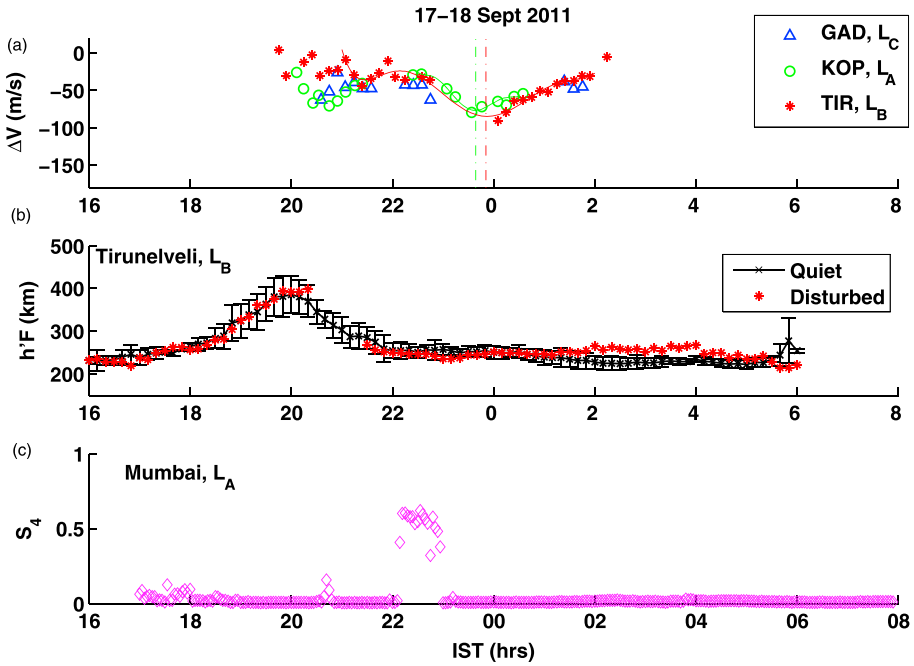

Figure 6. (a) Deviation in zonal irregularity drift, $\Delta V = V_D - \langle V_0 \rangle_Q$, as a function of IST observed at Tirunelveli, Gadanki, and Kolhapur. (b) Monthly quiet time average $h'F$ (black) and magnetically disturbed time $h'F$ (red) as a function of IST observed at Tirunelveli, L_B. (c) Time variation of S_4 at Mumbai, L_A on 17–18 September 2011. The vertical dash-dotted line in Figure 6a indicates the time of $|\Delta V|_{max}$. Due to weaker echoes from CADI ionosonde, $h'F$ values are not available between 20.5 and 21.5 IST on 17–18 September 2011.

The difference between disturbed time and monthly quiet time V_0 is computed for each station; i.e., $\Delta V = V_D - \langle V_0 \rangle_Q$. The variation of ΔV as a function of IST is shown in Figure 6a. To obtain the maximum deviation in zonal irregularity drift on disturbed day, a sixth-order polynomial is fitted to the variation of ΔV at Tirunelveli and Kolhapur. Due to lesser data points we have not fitted the sixth-order polynomial to ΔV at Gadanki. The maximum deviation in zonal irregularity drift, $|\Delta V|_{max}$, is found to be 84 m/s and 74 m/s at 23.9 and 23.6 IST, respectively, for Tirunelveli and Kolhapur, which are depicted in Figure 6a by vertical dash-dotted lines.

Figures 6b and 6c respectively show the average quiet time variation of $h'F$ with disturbed time $h'F$ at Tirunelveli and S_4 index observed at Mumbai, L_A. These observations confirm that no increase in F region is seen at Tirunelveli, L_B, that can assist the fresh generation of ESF at that longitude, whereas on 17–18 September 2011, scintillations are observed at Mumbai, L_A, only for a short duration which coincides with the time of generation of fresh ESF on longitude L_A. It suggests that the height of the freshly generated ESF irregularities over dip equator at longitude L_A was sufficient ($\geq$ 540 km) to map it down to Mumbai, which is located in equatorial anomaly region. It is worth noticing that the effect of DD on zonal irregularity drift is marginally smaller at off-equatorial station Kolhapur on longitude L_A as compared to that at equatorial station Tirunelveli on longitude L_B. The average effect on F region irregularity drift over an area that longitudinally-latitudinally covers 5.6°–8.9° is ~79 m/s, and it maximizes close to local midnight. The above discussed observations indicate that the effect of DD on V_0 is seen at all stations (i.e., L_A, L_B, and L_C), but the fresh generation of EPBs is triggered only in longitude A . The presence of scintillations at Mumbai (off-equatorial station over longitude L_A) during period of fresh generation indicates that the freshly generated irregularities were present at higher altitudes (>541 km) to map down to Mumbai. So we assume that the height of F region over L_A was high enough to initiate fresh generation of ESF irregularities, and it is attributed to the presence of crest of LSWS over that region.

5.2. Case 2: 6–7 April 2011

Here we discuss the observations on 6–7 April 2011, for Kolhapur L_A and Gadanki L_C. The observations on this day are depicted similar to those in Figures 5 and 6, and they are presented in Figures 7 and 8, respectively. Due to nonfunctioning of experiment, scintillation data are not available from Tirunelveli. Figure 7 shows the S_4, V_0, and $C_l(x_0, t_m)$ observed at (a) Gadanki, L_C and (b) Kolhapur, L_A. It may be noted that single quiet

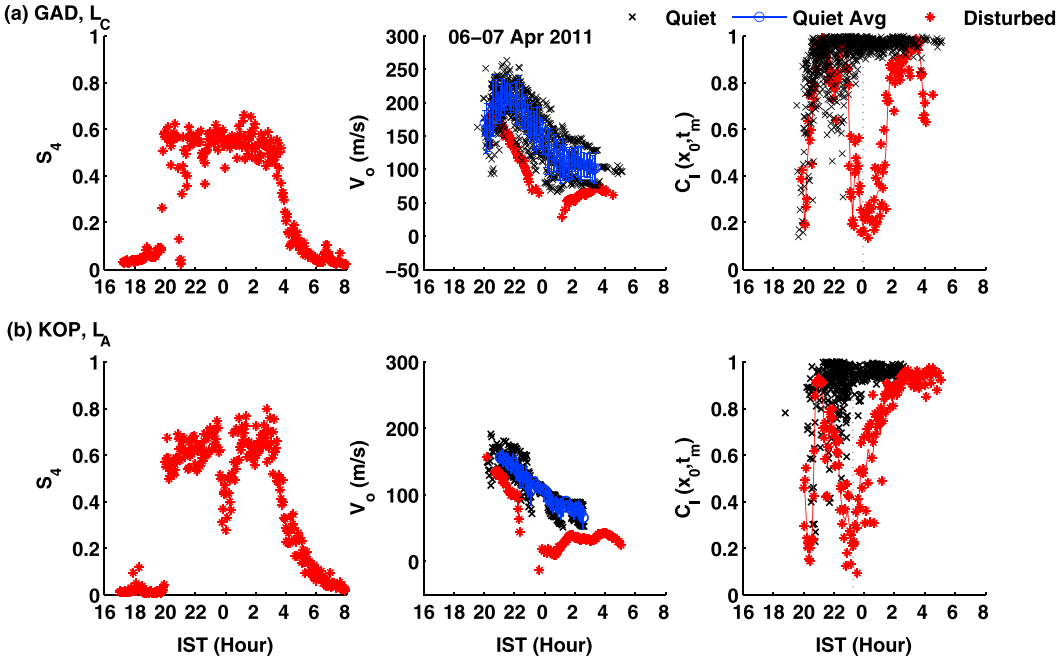

Figure 7. (left column) S_4; (middle column) quiet (black) and disturbed (red) time V_0, along with corresponding monthly quiet time average of V_0 (blue); (right column) quiet (black) and disturbed (red) time $C_I(x_0, t_m)$, as a function of IST for 6–7 April 2011 at observation stations (a) Gadanki, L_C and (b) Kolhapur, L_A.

day scintillation data were available for April 2011 for Gadanki. A single quiet day observation is statistically inadequate to estimate the monthly average pattern of V_0 and $C_I(x_0, t_m)$, and hence, we have taken scintillation observation during quiet days of March 2011. Average $F_{10.7}$ solar flux for March 2011 and April 2011 are 110 and 102, respectively. As solar flux is in close range to the average irregularity drift, V_0 for both equinoctial months can be assumed to have nearly the same day-to-day variations. Thus, the monthly quiet time pattern of V_0 and $C_I(x_0, t_m)$ displayed in Figure 7a is for March–April 2011. The low values of $C_I(x_0, t_m)$ are observed at both of these stations during 22–03 IST indicating the fresh generation of ESF irregularities at corresponding dip equatorial station on longitudes A and C. Furthermore, at both stations the disturbed time irregularity drift V_0 shows a large departure from their monthly quiet time variations that can be seen in Figure 7 (middle column). ΔV and its sixth-order polynomial fit are shown in Figure 8a for both stations. The maximum ΔV for Gadanki (L_C) and Kolhapur (L_A) are found to be 92 m/s and 87 m/s at 23.7 IST and 23.45 IST, respectively, which are indicated by vertical dash-dotted line in Figure 8a. For this case as well, the effect of DD on zonal irregularity drifts observed at Kolhapur, a station away from equator, is marginally smaller in comparison with the effects observed at Gadanki, a station close to equator. Overall, the average maximum effect on F region zonal plasma drift over observational area is found to be ~90 m/s around local midnight.

Figures 8b and 8c, respectively, shows the average quiet time variation of $h'F$ with disturbed time $h'F$ at Tirunelveli, and S_4 index observed at Mumbai, L_A for 6–7 April 2011. At Mumbai scintillations are observed during period of fresh generation. Generally, we expect increase in F layer height prior to the fresh generation of ESF irregularities as it assists the growth of RT instability. The base height of F region at L_B shows double hump structure with peak altitude of 481 km and 381 km at 19.83 IST and 21 IST, respectively. We assume that similar $h'F$ variation is present at L_A and L_C with variations due to presence of LSWS (±50–100 km). The second enhancement in $h'F$ at Tirunelveli occurred prior to the generation of fresh ESF irregularities, which initiated around 22 IST. Although the second increase in $h'F$ is relatively smaller, it is still well above the critical height of 300 km required for the generation of ESF irregularities [*Thampi et al.*, 2006]. In such case the RT plasma instability can be initiated with appropriate seed perturbation. Thus, these low-latitude ionospheric observations indicate that the magnetic activity-linked fresh generation of ESF is triggered at both longitudes A and C on 6–7 April 2011. We cannot conclude the fresh generation of ESF in longitude B due to nonavailability of data in this longitude on 6–7 April 2011.

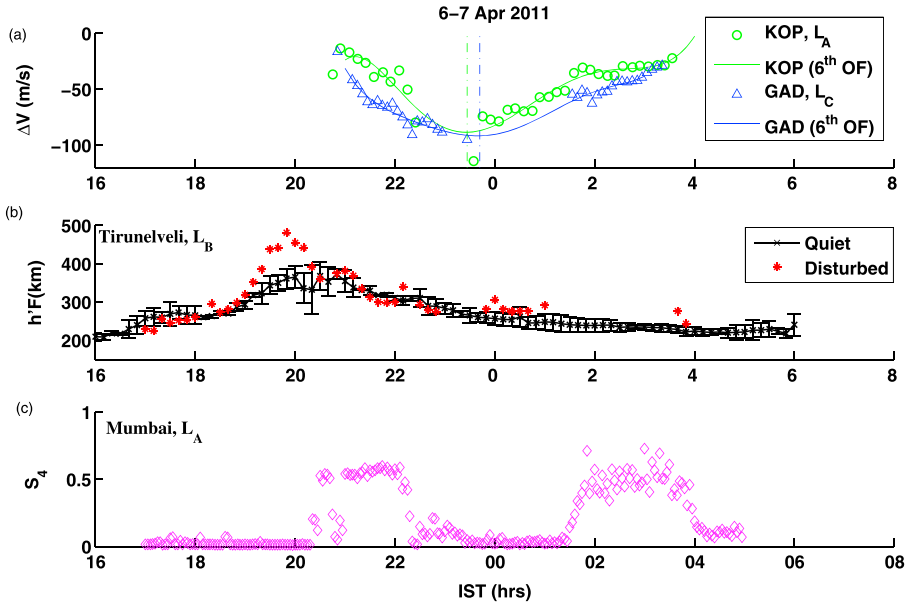

Figure 8. (a) Deviation in zonal irregularity drift, $\Delta V = V_D - \langle V_0 \rangle_Q$ as a function of IST observed at Gadanki and Kolhapur; (b) monthly quiet time average $h'F$ (black) and magnetically disturbed time $h'F$ (red) as a function of IST observed at Tirunelveli, L_B; (c) time variation of S_4 at Mumbai, L_A on 6–7 April 2011. The vertical dash-dotted line in Figure 8a indicates the time of $|\Delta V|_{max}$.

During nighttime ESF irregularities generally drift eastward. It is possible that ESF irregularities generated at equatorial station on L_A are drifting eastward and at later time observed at L_C. After 22 IST the drift speed for irregularities over Kolhapur are < 50 m/s. Assuming this possibility to be true, we find that irregularities moving with the drift speed of 50 m/s requires 2.77 h to cover a distance of 500 km. It indicates that signature of freshly generated EPBs at L_C should be observed after a delay of about 2.7 h. However, we have noticed freshly generated ESF irregularities at Gadanki and Kolhapur at nearly the same time. Thus, it is confirmed that ESF irregularities observed at Gadanki L_C are not the drifted one but they are generated locally.

5.3. Case 3: 9–10 September 2011

On 9–10 September we have observed very weak scintillations ($S_4 < 0.15$) at Gadanki L_C and Kolhapur L_A and hence could not compute V_0 and $C_l(x_0, t_m)$. In Figure 9 we have shown the observations from Tirunelveli. It should be noted that fresh ESF irregularities are observed during 00–02 IST that resulted in weak-moderate scintillations at Tirunelveli. Also, strongly westward zonal irregularity drift ($V_0 \approx -100$ m/s) is found to be present. The corresponding variation of ΔV as a function of time is shown in Figure 10a, which indicates the maximum deviation of 182 m/s at 01 IST. Recently, a large deviation of 227 m/s at around 22.33 IST in the irregularity drifts is reported [*Kakad et al.*, 2016], which so far is the largest deviation observed at Kolhapur. Figures 10b and 10c, respectively, shows the average quiet time variation of $h'F$ with disturbed time $h'F$ at Tirunelveli and S_4 index observed at Mumbai, Kolhapur, (L_A), and Gadanki (L_C). On this disturbed day, after suppression of usual postsunset prereversal enhancement (PRE), an increase in $h'F$ is initiated around 22 IST resulting in $h'F \sim 410$ km around 00 IST. It suggests the west to eastward turning of background electric field starting around 22 IST. The observed increase in $h'F$ is accompanied by the occurrence of freshly generated EPBs during 00–02 IST at Tirunelveli. Furthermore, very weak scintillations are observed at Gadanki, Mumbai, and Kolhapur only after 00 IST. These scintillations are so weak (<0.15) that we could not estimate V_0 and $C_l(x_0, t_m)$ information from these stations. It should be noted that increase in $h'F$ at L_B is very large indicating the presence of strong eastward DD electric field. In such situation the variations (increase/decrease) induced by the (crest/trough of) LSWS with vertical scales of 50–100 km become less significant as $h'F$ is elevated to higher altitudes. Thus, one can assume relatively less variation in $h'F$ at magnetic equator over longitudes L_A to L_C.

The base height of F region at Tirunelveli is depicted in Figure 10c, and it indicates that $h'F$ reached well above 400 km after 00 IST. As F peak has moved to significantly higher altitudes (≥506 km at 0.8 IST), only the lower part of freshly generated ESF irregularities might have been mapped to Gadanki, Kolhapur, or Mumbai.

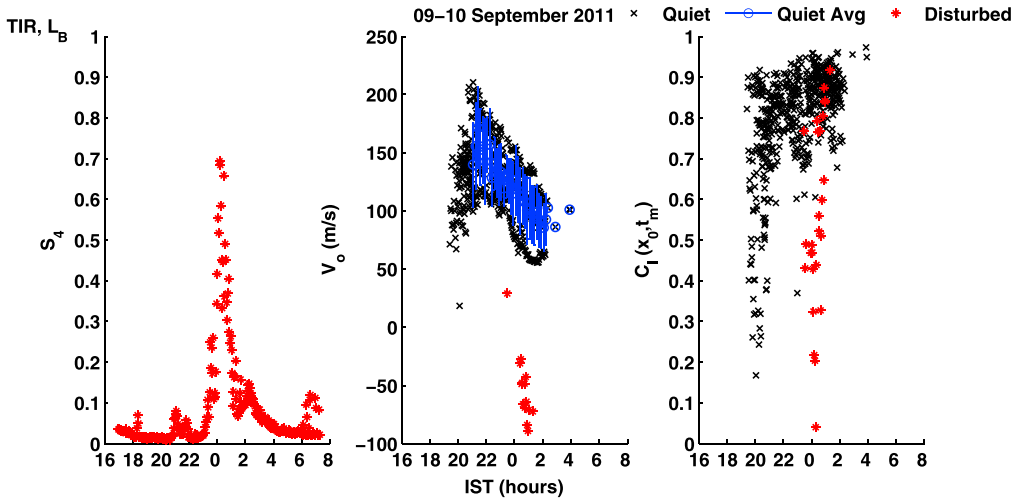

Figure 9. (left column) S_4; (middle column) quiet (black) and disturbed (red) time V_0, along with corresponding monthly quiet time average of V_0 (blue); (right column) quiet (black) and disturbed (red) time $C_l(x_0, t_m)$, as a function of IST for 9–10 September at Tirunelveli, L_B.

In such situation large-scale ESF irregularities, which are generally seen at lower altitudes can map down to these low-latitude stations. Theoretically, it is shown that the presence of large-scale ESF irregularities (i.e., with power spectral slope $m \geq 4$) gives rise to weaker S_4 as compared to small-scale irregularities when same density perturbations (ΔN) are associated with those irregularities [*Engavale and Bhattacharyya*, 2005; *Kakad et al.*, 2016]. Thus, the observed weak scintillations at low-latitude stations are consistent and can be understood in light of above mentioned theoretical model.

It should be noted that $h'F$ information is not available after 00.8 IST due to extremely weak echoes recorded by CADI ionosonde. In order to get information on height of irregularity layer, we carried out power spectral analysis of weak scintillation events particularly when V_0 estimates are available. We computed the height

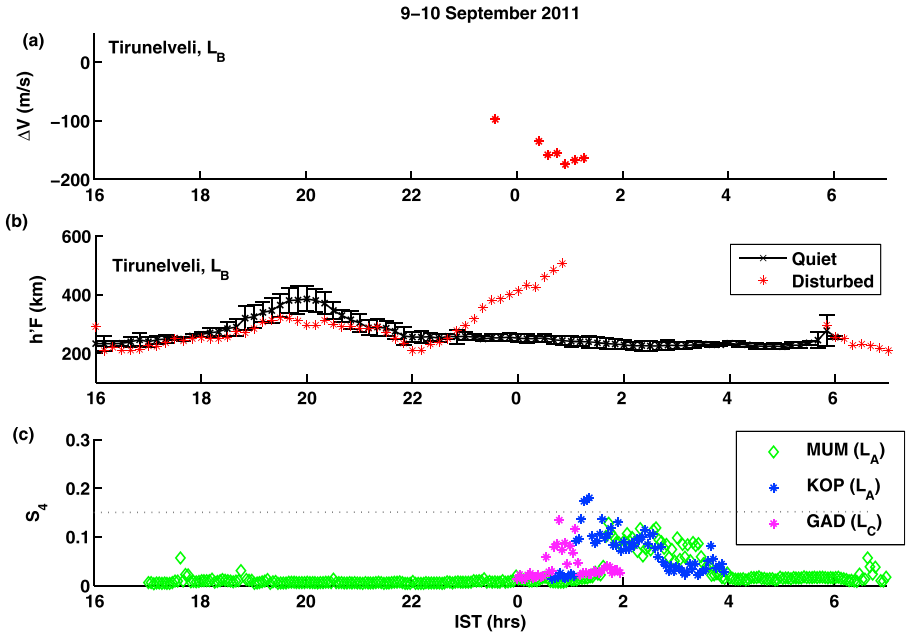

Figure 10. (a) Deviation in zonal irregularity drift, $\Delta V = V_D - \langle V_0 \rangle_Q$, as a function of IST observed at Tirunelveli, L_B; (b) monthly quiet time average $h'F$ (black) and magnetically disturbed time $h'F$ (red) as a function of IST observed at Tirunelveli, L_B; (c) time variation of S_4 at Kolhapur, Mumbai, and Gadanki on 9–10 September 2011. The horizontal dash-dotted line in Figure 10c indicates the $S_4 = 0.15$.

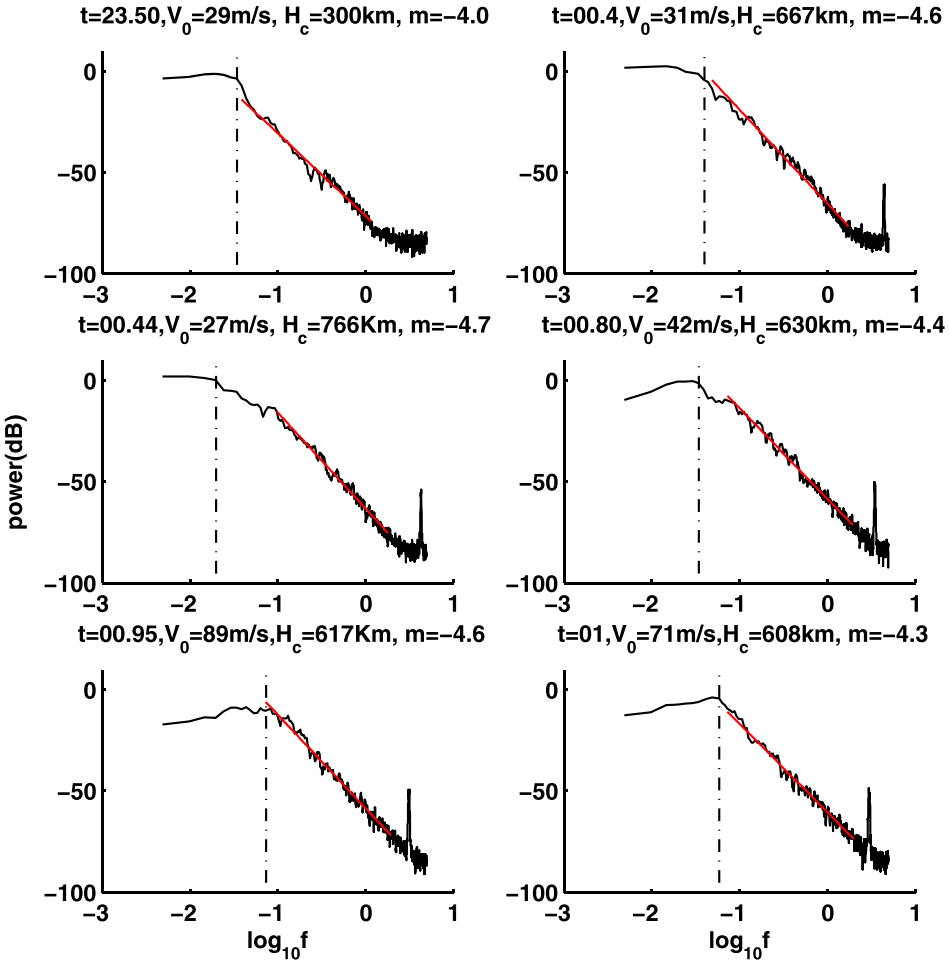

Figure 11. Power spectrum of weak scintillation events on 9–10 September 2011 at Tirunelveli. Occurrence time, V_0, height estimated from Fresnel frequency, and power spectral slope are mentioned in the corresponding subplots.

of irregularity layer using Fresnel frequencies as discussed in section 3. The examples of power spectrum are shown in Figure 11. It is found that the estimated average height of ESF irregularities lies in the range of 608–766 km. It further confirms the presence of freshly generated ESF at higher altitudes. Further, the power spectral index $m = 4–4.6$ indicates the presence of ESF structures with steeper power spectrum near equatorial *F* region peak.

6. Discussion

Scintillation observations for all three disturbed days discussed in previous section indicate that the zonal irregularity drift V_0 deviates significantly from their monthly average quiet time pattern, and it is evident at all stations. The magnitude of the maximum deviation in zonal irregularity drift ($|\Delta V|_{max}$) is slightly higher at dip equator as compared to that at low-latitude stations. Also, the maximum effect on V_0 occurs progressively later as the dip equator is approached. Earlier studies have reported that the usual eastward ambient zonal plasma drift turns to westward during periods of magnetic storms [*Fejer et al.*, 1991; *Fejer and Scherliess*, 1995; *Sutton et al.*, 2005], which is attributed to the process of disturbance dynamo (DD). During magnetically active periods large amount of charged particles enter into Earth's atmosphere at high latitudes through open magnetic field lines and precipitate therein. As a consequence conductivities and currents are enhanced at high-latitude ionosphere that results in increase in Joule energy and heats up the background neutrals. These modulated neutral winds blow from high to low latitude and set up a disturbance dynamo. During their propagation, they undergo deflection in westward direction due to coriolis force, which finally leads to a westward turning of zonal plasma drifts [*Abdu*, 2012].

As discussed in section 3, when the perturbation electric field associated with RT plasma instability is eroded, irregularities simply drift with the background plasma. Hence, the estimated V_0 represents the ambient zonal plasma drift given by $\vec{U} = -\vec{E_Z} \times \vec{B}/B^2$ [*Retterer*, 1999; *Valladares et al.*, 1996], where B is the horizontal component of the magnetic field at the station. The perturbation electric field linked with RT instability during periods of fresh generation of ESF is not decayed completely. In such cases the vertical component of perturbation electric field can still significantly contribute to estimated V_0 in addition to disturbed time ambient neutral wind U_D. Thus, the maximum deviation in irregularity zonal drift observed at these low-latitude stations is attributed to U_D and partly to the perturbation electric field linked with RT plasma instability at the time of fresh generation of ESF. It is important to note that for a given magnetic storm, the effect of DD at low-latitude F region zonal irregularity drift over an area having latitudinal (longitudinal) span of 8.9° (5.6°) is nearly the same.

Other important observation is the longitudinal differences in the occurrence of freshly generated ESF for these three magnetic storms that are studied here. On 17–18 September 2011 fresh ESF is observed in L_A only, and on 6–7 April 2011 the ESF is triggered in both L_A and L_C, whereas on 9–10 September 2011, the fresh ESF is observed at L_A, L_B, and L_C longitudes. Increase in F region height in the postsunset hours is favorable for the generation of ESF irregularities as lower ion-neutral collision frequencies at the enhanced F region altitude assist the growth rate of RT plasma instability. Even if favorable ambient conditions are available, the seed perturbation is required to trigger RT plasma instability in the postsunset hours. RT plasma instability takes few tens of minutes to grow and develop ESF irregularity structures through its nonlinear evolution. Thus, one can notice time delay between increase in F region height and the initiation of fresh generation of ESF for some cases as suggested by *Kakad et al.* [2012].

It should be noted that no increase in F region height over Tirunelveli is seen after 22 IST on 17–18 September 2011. At the same time, no fresh generation of ESF is observed over Tirunelveli on this day. On the other hand, large increase in F region height is seen on 9–10 September, when simultaneous fresh generation of ESF is observed. On this day the usual PRE is suppressed and F region started moving upward around 22 IST from 200 km to 506 km at around 00.8 IST. Similar F region height rise must be present at longitudes L_A and L_C as very weak scintillations are seen during 00–04 IST in those longitudes. It is likely that the enhanced $h'F$ helped the generation of fresh ESF around 00–02 IST on this day. On 6–7 April 2011, two enhancements in $h'F$, (i) 481 km at 19.8 IST and (ii) 381 km at 21 IST, are seen prior to the time of generation of fresh ESF. Even if the second increase in $h'F$ is relatively small, it is well above the critical height of 300 km required for the generation of ESF irregularities as suggested by *Thampi et al.* [2006]. Thus, with an appropriate seed perturbation at this height fresh ESF can be generated. The time difference between enhancement in $h'F$ and start of fresh ESF is about 1.1 h, and this delay is attributed to the growth time of RT plasma instability.

Finally, we need to understand the source and cause for such longitudinally varying occurrence of freshly generated ESF irregularities on these magnetically disturbed days. Electric fields associated with magnetic activity can be either eastward or westward, and it is the major source for the modulation of ambient quiet time electric fields in the ionosphere. The start time, and strength of magnetic activity, local time, longitude, ambient ionospheric, and magnetospheric conditions play an important role in determining its time variation and effectiveness in the Earth's ionosphere. Past studies have shown that the DD electric field turns from west-east around local midnight, and thus, F region can be raised to higher altitude around midnight. With an appropriate seed perturbation the RT plasma instability can be triggered to give rise to nonlinearly evolved EPBs and associated irregularities. Disturbed time electric field varies with space (longitude and latitude) and time. Simulation results suggest that DD electric field is eastward around local midnight, and it does not change rapidly over a smaller longitudinal belt having a span of few degrees (i.e., over <5.6°) at low-latitude stations [*Huang*, 2013]. Thus, the base height of F region is not expected to vary significantly over this small longitudinal belt. Hence, one does not expect the variability in the occurrence of fresh generation of ESF within such narrow longitudinal belt. It is known that several upwelling in electron density can often exist at the bottomside of F region in the form of wave referred to as large-scale wave structures (LSWS) [*Tsunoda and White*, 1981]. Studies in recent past have shown that the LSWS evolves as a standing wave with insignificant zonal propagation [*Tsunoda and Ecklund*, 2007; *Patra et al.*, 2013; *Joshi*, 2016]. Also, It is demonstrated that these LSWS remain present in the ionosphere even after the generation of the plasma bubble, and its signature can be seen in radar maps as the bottomside modulation of F region [*Kelley et al.*, 1981; *Patra et al.*, 2015]. If the DD electric field associated with magnetic activity is eastward, then it can lift F region upward around midnight. However, the presence of the LSWS can modulate the F region base height significantly. The vertical scales

Table 3. Summary of Results for Three Magnetic Storm Studied Here Are Presented[a]

	Fresh ESF (Y/N)			$\lvert\Delta V\rvert_{max}$ ($t_{\lvert\Delta V\rvert_{max}}$)			$\Delta T = \langle T_{sunset}\rangle - T_D$
	L_A	L_B	L_C	L_A	L_B	L_C	(h)
Case 1	Yes	No	No	74 m/s (23.6 IST)	84 m/s (23.9 IST)	–	4.7
Case 2	Yes	–	Yes	87 m/s (23.45 IST)	–	91.6 m/s (23.7 IST)	3.0
Case 3	Yes	Yes	Yes	–	182 m/s (01 IST)	–	0.0

[a]Occurrence of freshly generated ESF irregularities (in column 1), maximum deviation in zonal plasma drift, and its time are listed for three longitudes L_A, L_B, and L_C (in column 2). The time difference between start time of magnetic activity and average sunset time ΔT (in column 3).

of these structures are around 50–100 km, whereas the zonal extent is less than 300 km [*Tsunoda*, 2015]. It suggests that the presence of LSWS can cause increase/decrease of the order of few hundred kilometers in the base height of *F* region closer to crest/trough of this wave structure. Thus, if DD electric field in the later part of the night (around midnight) has to manifest in the form of fresh generation of ionospheric irregularities, it will happen only at the crest of the LSWS. Thus, the fresh generation of ESF irregularities associated with DD will not happen everywhere within a narrow longitudinal belt of 5.6° as found in present study. Earlier studies have shown that the these LSWS is found to have a higher correlation with the occurrence of EPBs, which grows on the crest (upwelling) of these structures [*Singh et al.*, 1997; *Thampi et al.*, 2009; *Li et al.*, 2012]. Thus, the presence of LSWS at the bottomside of *F* region during periods of generation of fresh generation around midnight can possibly explain the observed longitudinal variability in the occurrence of fresh ESF on disturbed days.

7. Summary and Conclusions

In the present study we used VHF amplitude scintillation data from a network of spaced receivers operational at low-latitude stations in Indian longitude. The effect of magnetic activity on low-latitude *F* region are discussed for three magnetic storm occurring in 2011 that are having nearly similar-type characteristics except the start time. The difference between the start time of magnetic storms and average local sunset is approximately $\Delta T = 4.7$, 3, and 0 h for 17–18 September, 6–7 April, and 9–10 September 2011, respectively. The magnetic activity-linked effects are examined in context of (i) zonal irregularity drifts and (ii) occurrence of freshly generated ESF. The results from present study are summarized in Table 3. For all three cases, it is found that effects caused by magnetic storms on *F* region zonal plasma drifts are dominantly seen during 22–04 IST at all observational stations that latitudinally (longitudinally) covers an area of 8.9° (5.6°). These effects are associated with a short-term DD electric field as they are evident nearly 4–10 h after the initiation of magnetic activity. The maximum westward deviation observed in zonal irregularity drift is only marginally smaller at low-latitude stations Kolhapur/Gadanki as compared to dip equatorial station Tirunelveli for a given magnetic storm. Moreover, it is observed that the DD effects seen at low-latitude *F* region zonal irregularity drifts becomes more pronounced as ΔT decrease. It should be noted that the average Joule energy deposited at high latitudes from start time of magnetic storm (T_D) till the time of maximum effect in V_0 (i.e T_{max}) are 4.25 J, 3.54 J, and 3.70 J, respectively, for 17–18 September, 6–7 April, and 9–10 September 2011, respectively. Although these Joule energy inputs are in close range, the magnitude of maximum deviation in zonal irregularity drift ($\lvert\Delta V\rvert_{max}$) varies in the range of 74–84 m/s, 87–92 m/s, and 182 m/s, respectively, for these cases. The time difference between the start time of magnetic activity and the time of sunset (ΔT) is found to play a role in determining DD electric field-linked effects at low-latitude *F* region, which might be arising due to changes in ionospheric conductivity from day to dusk sector. Further, the occurrence of fresh ESF is mainly observed around midnight. Although DD electric field linked with magnetic activity is expected to be of nearly same strength and direction in a narrow longitudinal belt of 5.6° at a given time, the present study shows the variability in the occurrence of fresh generation of ESF within such a narrow longitudinal zone. This is attributed to the presence of LSWS at the bottomside of *F* region at the time of their initiation, as EPBs

are more likely to be generated in the vicinity of upwelling of the LSWS. When the onset of magnetic storm coincides with local sunset the midnight occurrence of EPBs are reported in earlier studies [*Chakrabarty et al.*, 2006; *Tulasi Ram et al.*, 2008]. The present study bring out the features of longitudinal and latitudinal variability in the occurrence of freshly generated ESF irregularities and zonal irregularity drift over Indian longitude for three similar-type magnetic storms.

Acknowledgments
We thank Sripathi, IIG for providing ionosonde data. Thanks are due to K. Jeeva, K.U. Nair, Ananthi, Rupesh, and S. Banola for their technical support on the scintillation experiment. We thank http://wdc.kugi.kyoto-u.ac.jp/ and http://cdaweb.sci.gsfc.nasa.gov/index.html/ for geomagnetic activity indices and interplanetary parameters utilized in the study. A.B. acknowledges Indian National Science Academy for an INSA senior scientist position at IIG.

References

Abdu, M. A. (2012), Equatorial spread *F*/plasma bubble irregularities under storm time disturbance electric fields, *J. Atmos. Terr. Phys.*, *75*, 44–56, doi:10.1016/j.jastp.2011.04.024.

Abdu, M. A., I. S. Batista, and J. H. A. Sobral (1992), A new aspect of magnetic declination control of equatorial spread *F* and *F*-region dynamo, *J. Geophys. Res.*, *97*, 14,897–14,904.

Abdu, M. A., J. H. Sastri, J. MacDougall, I. S. Batista, and J. H. A. Sobral (1997), Equatorial disturbance dynamo electric field longitudinal structure and spread *F*: A case study from GUARA/EITS campaigns, *Geophys. Res. Lett.*, *24*(13), 1707–1710.

Akasofu, S. (1981), Energy coupling between the solar wind and the magnetosphere, *Space Sci. Rev.*, *28*, 121–190, doi:10.1007/BF00218810.

Blanc, M., and A. D. Richmond (1980), The ionospheric disturbance dynamo, *J. Geophys. Res.*, *85*, 1669–1686.

Basu, S., S. Basu, E. Kudeki, H. P. Zeningonul, M. A. Biondi, and J. W. Meriwether (1991), Zonal irregularity drifts and neutral winds measured near the magnetic equator in Peru, *J. Atmos. Sol. Terr. Phys.*, *53*(8), 743–747.

Basu, S., et al. (1996), Scintillations, plasma drifts, and neutral winds in the equatorial ionosphere after sunset, *J. Geophys. Res.*, *101*(A12), 26,795–26,809.

Bhattacharyya, A., S. J. Franke, and K. C. Yeh (1989), Characteristic velocity of equatorial *F* region irregularities determined from spaced receiver scintillation data, *J. Geophys. Res.*, *94*(A9), 11,959–11,969.

Bhattacharyya, A., S. Basu, K. M. Groves, C. E. Valladares, and R. Sheehan (2001), Dynamics of equatorial *F* region irregularities from spaced receiver scintillation observations, *Geophys. Res. Lett.*, *28*(1), 119–122.

Bhattacharyya, A., S. Basu, K. M. Groves, C. E. Valladares, and R. Sheehan (2002), Effect of magnetic activity on the dynamics of equatorial *F* region irregularities, *J. Geophys. Res.*, *107*(A12), 1489, doi:10.1029/2002JA009644.

Bhattacharyya, A., B. Kakad, S. Sripathi, K. Jeeva, and K. U. Nair (2014), Development of intermediate scale structure near the peak of the *F* region within an equatorial plasma bubble, *J. Geophys. Res. Space Physics*, *119*, 3066–3076, doi:10.1002/2013JA019619.

Bhattacharyya, A., B. Kakad, P. Gurram, S. Sripathi, and S. Sunda (2017), Development of intermediate-scale structure at different altitudes within an equatorial plasma bubble: Implications for L-band scintillations, *J. Geophys. Res. Space Physics*, *122*, 1015–1030, doi:10.1002/2016JA023478.

Brigg, B. H. (1984), The analysis of spaced sensor records by correlation techniques, in *Middle Atmosphere Program, Handbook for MAP*, vol. 13, edited by R. A. Vincent, pp. 166–186, Int. Counc. of Sci. Unions, Paris.

Burke, W. J., L. C. Gentile, C. Y. Huang, C. E. Valladares, and S. Y. Su (2004), Longitudinal variability of equatorial plasma bubbles observed by DMSP and ROCSAT-1, *J. Geophys. Res.*, *109*, A12301, doi:10.1029/2004JA010583.

Chakrabarty, D., R. Sekar, R. Narayanan, A. K. Patra, and C. V. Devasia (2006), Effects of interplanetary electric field on the development of an equatorial spread *F* event, *J. Geophys. Res.*, *111*, A12316, doi:10.1029/2006JA011884.

Engavale, B., and A. Bhattacharyya (2005), Spatial correlation function of intensity variations in the ground scintillation pattern produced by equatorial spread *F* irregularities, *Indian J. Radio Space Phys.*, *34*, 23–32.

Engavale, B., K. Jeeva, K. U. Nair, and A. Bhattacharyya (2005), Solar flux dependence of coherence scales in scintillation patterns produced by ESF irregularities, *Ann. Geophys.*, *23*, 3261–3266.

Fejer, B. G., and L. Scherliess (1995), Time dependent response of equatorial ionospheric electric fields to magnetospheric disturbances, *Geophys. Res. Lett.*, *22*, 851–854.

Fejer, B. G., R. W. Spiro, R. A. Wolf, and J. C. Foster (1990), Latitudinal variation of perturbation electric fields during magnetically disturbed periods: 1986 SUNDIAL observations and model results, *Ann. Geophys.*, *8*, 441–454.

Fejer, B. G., E. R. dePaula, S. A. Gonzalez, and R. F. Woodman (1991), Average vertical and zonal *F* region plasma drifts over Jicamarca, *J. Geophys. Res.*, *96*(A8), 13,901–13,906, doi:10.1029/91JA01171.

Heelis, R. A., P. C. Kendall, R. J. Moffett, and D. W. Windle (1974), Electrical coupling of the *E*- and *F*-regions and its effect on *F*-region drifts and winds, *Planet. Space Sci.*, *22*, 743–756.

Huang, C. M. (2013), Disturbance dynamo electric fields in response to geomagnetic storms occurring at different universal times, *J. Geophys. Res. Space Physics*, *118*, 496–501, doi:10.1029/2012JA018118.

Huang, C. M., A. D. Richmond, and M. Q. Chen (2005), Theoretical effects of magnetic activity on low latitude ionospheric electric fields, *J. Geophys. Res.*, *110*, A05312, doi:10.1029/2004JA010994.

Huang, C.-S., and M. C. Kelley (1996), Nonlinear evolution of equatorial spread *F*: 1. On the role of plasma instabilities and spatial resonance associated with gravity wave seeding, *J. Geophys. Res.*, *101*(A1), 283–292, doi:10.1029/95JA02211.

Joshi, L. M. (2016), LSWS linked with the low-latitude E_s and its implications for the growth of the R-T instability, *J. Geophys. Res. Space Physics*, *121*, 6986–7000, doi:10.1002/2016JA022659.

Joshi, L. M., A. K. Patra, T. K. Pant, and S. V. B. Rao (2013a), On the nature of low latitude E_s influencing the genesis of equatorial plasma bubble, *J. Geophys. Res. Space Physics*, *118*, 524–532, doi:10.1029/2012JA018122.

Joshi, L. M., A. K. Patra, and S. V. B. Rao (2013b), Low latitude E_s capable of controlling the onset of equatorial spread *F*, *J. Geophys. Res. Space Physics*, *118*, 1170–1179, doi:10.1002/jgra.50189.

Joshi, L. M., S. Balwada, T. K. Pant, and S. G. Sumod (2015), Investigation on *F* layer height rise and equatorial spread *F* onset time: Signature of standing large-scale wave, *Space Weather*, *13*, 211–219, doi:10.1002/2014SW001129.

Kakad, B., K. Jeeva, K. U. Nair, and A. Bhattacharyya (2007), Magnetic activity linked generation of nighttime equatorial spread *F* irregularities, *J. Geophys. Res.*, *112*, A07311, doi:10.1029/2006JA012021.

Kakad, B., D. Tiwari, and T. K. Pant (2011), Study of disturbance dynamo effects at nighttime equatorial *F* region in Indian longitude, *J. Geophys. Res.*, *116*, A12318, doi:10.1029/2011JA016626.

Kakad, B., C. K. Nayak, and A. Bhattacharyya (2012), Power spectral characteristics of ESF irregularities during magnetically quiet and disturbed days, *J. Atmos. Sol. Terr. Phys.*, *81*, 41–49, doi:10.1016/j.jastp.2012.04.008.

Kakad, B., P. Gurram, P. N. B. Tripura Sundari, and A. Bhattacharyya (2016), Structuring of intermediate scale equatorial spread *F* irregularities during intense geomagnetic storm of solar cycle 24, *J. Geophys. Res. Scape Physics*, *121*, 7001–7012, doi:10.1002/2016JA022635.

Krall, J., J. D. Huba, and D. C. Fritts (2013), On the seeding of equatorial spread *F* by gravity waves, *Geophys. Res. Lett.*, *40*, 661–664, doi:10.1002/grl.50144.
Kelley, M. C. (1989), *The Earth's Ionosphere and Electrodynamics and Plasma Physics*, Academic Press, New York.
Kelley, M. C., M. F. Larsen, C. LaHoz, and J. P. McClure (1981), Gravity wave initiation of equatorial spread *F*: A case study, *J. Geophys. Res.*, *86*(A11), 9087–9100, doi:10.1029/JA086iA11p09087.
Kil, H., P. M. Kintner, E. R. de Paula, and I. J. Kantor (2002), Latitudinal variations of scintillation activity and zonal plasma drifts in South America, *Radio Sci.*, *37*(1), 1006, doi:10.1029/2001RS002468.
Ledvina, B. M., P. M. Kintner, and E. R. de Paula (2004), Understanding spaced-receiver zonal velocity estimation, *J. Geophys. Res.*, *109*, A10306, doi:10.1029/2004JA010489.
Li, G., B. Ning, M. A. Abdu, W. Wan, and L. Hu (2012), Precursor signatures and evolution of post-sunset equatorial spread-*F* observed over Sanya, *J. Geophys. Res.*, *117*, A08321, doi:10.1029/2012JA017820.
Martinis, C. R., M. J. Mendillo, and J. Aarons (2005), Toward a synthesis of equatorial spread *F* onset and suppression during magnetic storms, *J. Geophys. Res.*, *110*, A07306, doi:10.1029/2003JA010362.
Maruyama, N., A. D. Richmond, T. J. Fuller-Rowell, M. V. Codrescu, S. Sazykin, F. R. Toffoletto, R. W. Spiro, and G. H. Millward (2005), Interaction between direct penetration and disturbance dynamo electric fields in the storm-time equatorial ionosphere, *Geophys. Res. Lett.*, *32*, L17105, doi:10.1029/2005GL023763.
Nishioka, M., A. Saito, and T. Tsugawa (2008), Occurrence characteristics of plasma bubble derived from global ground-based GPS receiver networks, *J. Geophys. Res.*, *113*, A05301, doi:10.1029/2007JA012605.
Patra, A. K., A. Taori, P. P. Chaitanya, and S. Sripathi (2013), Direct detection of wavelike spatial structure at the bottom of the *F* region and its role on the formation of equatorial plasma bubble, *J. Geophys. Res. Space Physics*, *118*, 1196–1202, doi:10.1002/jgra.50148.
Patra, A. K., P. Srinivasulu, P. P. Chaitanya, M. D. Rao, and A. Jayaraman (2015), First results on low latitude *E* and *F* region irregularities obtained using the Gadanki Ionospheric Radar Interferometer, *J. Geophys. Res. Space Physics*, *119*, 10,276–10,293, doi:10.1002/2014JA020604.
Park, J., H. Luhr, B. G. Fejer, and K. W. Min (2010), Duskside *F*-region dynamo currents: Its relationship with prereversal enhancement of vertical plasma drift, *Ann. Geophys.*, *28*, 2097–2101.
Retterer, J. M. (1999), Theoretical model for fast equatorial bubbles, in *Proceeding of Ionospheric Effects Symposium*, edited by J. M. Goodman, p. 688, Natl. Tech. Inf. Serv., Springfield, Alexandria, Va.
Richmond, A. D., C. Peymirat, and R. G. Roble (2003), Long-lasting disturbances in the equatorial ionospheric electric field simulated with a coupled magnetosphere-ionosphere-thermosphere model, *J. Geophys. Res.*, *108*(A3), 1118, doi:10.1029/2002JA009758.
Sastri, J. H. (1999), Post-midnight onset of spread-*F* at Kodaikanal during the June solstice of solar minimum, *Ann. Geophys.*, *17*, 1111–1115.
Scherliess, L., and B. G. Fejer (1997), Strom time dependence of equatorial disturbance dynamo zonal electric fields, *J. Geophys. Res.*, *102*, 24,037–24,046.
Singh, S., F. S. Johnson, and R. A. Power (1997), Gravity wave seeding of equatorial plasma bubbles, *J. Geophys. Res.*, *102*, 7399–7410.
Spiro, R. W., R. A. Wolf, and B. G. Fejer (1988), Penetration of high-latitude electric field effects to low latitude during SUNDIAL 1984, *Ann. Geophys.*, *6*, 39–50.
Sutton, E. K., J. M. Forbes, and R. S. Nerem (2005), Global thermospheric neutral density and wind response to the severe 2003 magnetic storms from CHAMP accelerometer data, *J. Geophys. Res.*, *110*, A09S40, doi:10.1029/2004JA010985.
Thampi, S. V., S. Ravindran, T. K. Pant, C. V. Devasia, P. Sreelatha, and R. Sridharan (2006), Deterministic prediction of post-sunset ESF based on the strength and asymmetry of EIA from ground based TEC measurements: Preliminary results, *Geophys. Res. Lett.*, *33*, L13103, doi:10.1029/2006GL026376.
Thampi, S. V., M. Yamamoto, R. T. Tsunoda, Y. Otsuka, T. Tsugawa, J. Uemoto, and M. Ishii (2009), First observations of large-scale wave structure and equatorial spread F using CERTO radio beacon on the C/NOFS satellite, *Geophys. Res. Lett.*, *36*, L18111, doi:10.1029/2009GL039887.
Tsunoda, R. T. (1985), Control of the seasonal and longitudinal occurrence of equatorial scintillations by the longitudinal gradient in integrated *E* region Pedersen conductivity, *J. Geophys. Res.*, *90*(A1), 447–456, doi:10.1029/JA090iA01p00447.
Tsunoda, R. T. (2005), On the enigma of day-to-day variability in equatorial spread *F*, *Geophys. Res. Lett.*, *32*, L08103, doi:10.1029/2005GL022512.
Tsunoda, R. T. (2012), A simple model to relate ionogram signatures to large-scale wave structure, *Geophys. Res. Lett.*, *39*, L18107, doi:10.1029/2012GL053179.
Tsunoda, R. T. (2015), Upwelling: A unit of disturbance in equatorial spread *F*, *Prog. Earth Planet. Sci.*, *2*, 9, doi:10.1186/s40645-015-0038-5.
Tsunoda, R. T., and B. R. White (1981), On the generation and growth of equatorial backscatter plumes: 1. Wave structure in the bottomside *F* layer, *J. Geophys. Res.*, *86*, 3610–3616, doi:10.1029/JA086iA05p03610.
Tsunoda, R. T., and W. L. Ecklund (2007), On the post sunset rise of the equatorial *F* layer and superposed upwellings and bubbles, *Geophys. Res. Lett.*, *34*, L04101, doi:10.1029/2006GL028832.
Tulasi Ram, S., P. V. S. Rama Rao, D. S. V. V. D. Prasad, K. Niranjan, S. Gopi Krishna, R. Sridharan, and S. Ravindran (2008), Local time dependent response of postsunset ESF during magnetic storms, *J. Geophys. Res.*, *113*, A07310, doi:10.1029/2007JA012922.
Tulasi Ram, S., M. Yamamoto, R. T. Tsunoda, H. D. Chau, T. L. Hoang, B. Damtie, M. Wassaie, C. Y. Yatini, T. Manik, and T. Tsugawa (2014), Characteristics of large-scale wave structure observed from African and Southeast Asian longitudinal sectors, *J. Geophys. Res. Space Physics*, *119*, 2288–2297, doi:10.1002/2013JA019712.
Valladares, C. E., R. Sheehan, S. Basu, H. Kuenzler, and J. Espinoza (1996), The multi-instrumented studies of equatorial thermosphere aeronomy scintillation system: Climatology of zonal drifts, *J. Geophys. Res.*, *101*(A12), 26,839–26,850.
Valladares, C. E., J. W. Meriwether, R. Sheehan, and M. A. Biondi (2002), Correlative study of neutral winds and scintillation drifts measured near the magnetic equator, *J. Geophys. Res.*, *107*(A7), 1112, doi:10.1029/2001JA000042.
Wernik, A. W., C. H. Liu, and K. C. Yeh (1983), Modeling of spaced-receiver scintillation measurements, *Radio Sci.*, *18*(5), 743–764.
Yeh, K. C., and C. H. Liu (1982), Radio wave scintillations in the ionosphere, *Proc. IEEE*, *70*, 324–360.
Yeh, K. C., H. Soicher, C. H. Liu, and E. Bonelli (1979), Ionospheric bubbles observed by the Faraday rotation method at Natal, Brazil, *Geophys. Res. Lett.*, *6*, 473–475, doi:10.1029/GL006i006p00473.
Zhu, Z., J. Lan, W. Luo, F. Sun, K. Chen, and S. Chang (2015), Statistical characteristics of ionogram spread-*F* and satellite traces over a Chinese low latitude station Sanya, *Adv. Space Res.*, *56*, 1911–1921, doi:10.1016/j.asr.2015.03.038.